Catal Lett (2010) 134:63–71
DOI 10.1007/s10562-009-0232-4

Anchoring of Chiral Manganese(III) Salen Complex onto Organo Clay and Porous Clay Heterostructure and Catalytic Activity in Alkene Epoxidation

Iwona Kuźniarska-Biernacka · Ana R. Silva · Ana P. Carvalho · João Pires · Cristina Freire

Received: 6 August 2009 / Accepted: 19 November 2009 / Published online: 1 December 2009

Abstract The chiral Mn(III) salen complex (C1) was immobilised onto a natural clay (BEN) and a porous clay heterostructure (PCH) functionalised with 3-aminopropyltriethoxysilane (APTES). FTIR, XPS and Mn chemical analysis confirm the C1 anchorage in both materials, but with higher efficiency in BEN_APTES clay. The catalytic activity of C1@BEN_APTES and C1@PCH_APTES, was assessed in the epoxidation of styrene (sty) and ∝-methylstyrene (∝-Mesty) using NaOCl and *m*-chloroperoxybenzoic acid (*m*-CPBA)/N-methylmorpholine-N-oxide (NMO). Both materials behave as moderate catalysts, show high epoxide selectivity but low enantiomeric excesses. In the case of sty epoxidation with *m*-CBPA/NMO the C1@PCH_APTES catalyst showed the highest catalytic activity, whereas in ∝-Mesty epoxidation, the C1@PCH_APTES catalyst, although leading to lower substrate conversion than the BEN analogue, presented the lowest complex leaching. In all cases, the oxidant NaOCl had some destructive effect in the hybrid catalysts, highlighting the importance of a careful choice of catalyst and oxidant system.

Keywords Mn(salen) complexes · Covalent immobilisation · Clay based materials · Heterogeneous epoxidation · Alkenes

1 Introduction

Chiral Mn(III) salen transition metal complexes have become a matter of long-term interest due to their scope of applications as homogeneous catalysts in asymmetric epoxidation of unfunctionalised alkenes. The separation and recycling of homogeneous catalysts is problematic, making the entire catalytic process economically nonviable for industrial processes. Therefore, the heterogenisation of homogeneous catalysts has become an important strategy to obtain supported catalysts that retain the homogeneous catalytic sites with the advantages of easy separation and recycling. Up to date many studies on the heterogenisation of chiral Mn(III) salen complexes have been performed. These include Mn complex immobilisation onto organic polymers [1–3] and inorganic porous solids [4–13]. Catalytic studies with immobilised chiral Mn(III) salen complexes revealed that the local environment inside the pores and the pore size of the supports affect the enantioselectivity of the catalysts in epoxidation reactions. On the other hand, and concerning the properties of the porous supports, their chemical stability in the catalytic reaction conditions is also an important issue. In fact, particularly in oxidation reactions, some oxidants may have a pernicious effect on

Electronic supplementary material The online version of this article (doi:10.1007/s10562-009-0232-4) contains supplementary material, which is available to authorized users.

I. Kuźniarska-Biernacka · A. R. Silva · C. Freire (✉)
REQUIMTE, Departamento de Química, Faculdade de Ciências, Universidade do Porto, Rua do Campo Alegre, 4169-007 Porto, Portugal
e-mail: acfreire@fc.up.pt

A. P. Carvalho · J. Pires
Departamento de Química e Bioquímica and CQB, Faculdade de Ciências, Universidade de Lisboa, Ed. C8, Campo Grande, 1749-016 Lisbon, Portugal

I. Kuźniarska-Biernacka
Centro de Química, Universidade do Minho, Campus de Gualtar, 4710-057 Braga, Portugal

A. R. Silva
CICECO, Universidade de Aveiro, Campus Universitário de Santiago, 3810-193 Aveiro, Portugal

Scheme 1 Anchoring methods followed in the immobilisation of C1 onto clay based materials

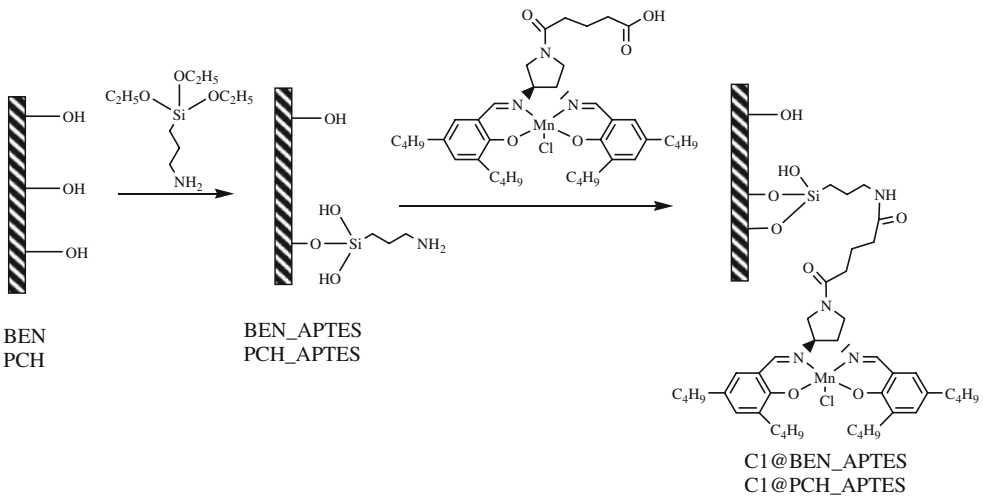

the stability of the support structure, which may lead to its partial collapse [14].

Recent studies on clay based materials have been focused in the preparation of stable materials with larger pores than those of the more traditional zeolites. This is at least the case when the conventional procedures of pillaring are employed, that is, by exchanging a swelling clay with an oligomeric cation and calcinating the resulting material to produce a pillared clay (PILC) [15]. In the last decade, and particularly in a limited number of studies, a different approach was followed to obtain porous materials from clays, by combining the pillaring and the templating approaches [16–18]. The obtained solids are usually referred to as porous clays heterostructures (PCHs), and have specific surface areas in the range of 700–1,000 $m^2\ g^{-1}$ and high thermal stability, being prepared by surfactant-directed assemblies of silica in the two dimensional interlayer spacing of clays. In the first step of the PCHs preparation, the clay is expanded by exchange with an ionic surfactant, such as cetyltrimethylammonium bromide (CTAB), to allow an easier access to the interlayer region. A neutral amine is then intercalated, together with a silicate source such as tetraethylorthosilicate (TEOS). The silicate source partially displaces the neutral amine, and the interactions between the surfactants and the silicate ions are believed to give rise to micellar assemblies in the clay interlayer space. The organic components are then removed by calcination. Up to now a large variety of organo-clays have been synthesised using different surfactants and their structures have been characterised using various techniques, [19, 20] including powder X-ray diffraction (PXRD), Fourier transform infrared spectroscopy (FTIR) and X-ray photoelectron spectroscopy (XPS).

Herein, we describe the immobilisation by covalent bonding of a chiral Mn(III) salen complex (C1) onto a natural clay (BEN) and a PCH using APTES as the reactive surface modifier, Scheme 1. To allow the maximum conformational mobility of the complex which is necessary to obtain a high level of asymmetric induction, the grafting was performed through a pendant arm of the Mn complex imine bridge. After the physicochemical characterisation, the heterogeneous catalysts were tested in the epoxidation of styrene and ∝-methylstyrene using NaOCl and *m*-CPBA/NMO as oxygen sources.

2 Experimental

2.1 Solvents and Reagents

The compounds, 3-aminopropyltriethoxysilane (APTES), 1-hydroxybenzotriazole hydrate, N,N′-dimethylformamide, diisopropylethylamine, 1,3-diisopropylcarbodiimine, chloroform, styrene (sty), ∝-methylstyrene (∝-Mesty), chloroperoxybenzoic acid (*m*-CPBA), N-methylmorpholine-N-oxide (NMO) and NaOCl were from Aldrich. Dichloromethane and toluene (UV–Vis spectroscopic grade) were from Romil. The multi-step synthesis of salen ligand and its Mn(III) complex have been reported elsewhere [21].

2.2 Preparation of Materials

A portuguese clay (BEN) was used as starting material; its characterisation has been reported elsewhere; [22] the preparation and characterisation of the PCH has also been previously described in ref [18].

2.2.1 APTES-Modification of Supporting Materials

The APTES-functionalisation of BEN and PCH was performed by the following procedure: 1.6 g of BEN or PCH was added to a solution of 0.4 cm^3 (1.7 mmol) of APTES and 15 cm^3 of toluene and refluxed for 48 h in argon atmosphere. The obtained materials, denoted as

BEN_APTES and PCH_APTES, were separated by centrifugation, washed with dichloromethane and finally dried at 120 °C for 24 h.

2.2.2 *Immobilisation of C1 Onto Organo-Modified Supports*

The immobilisation of C1 in the APTES-modified materials was performed by the following method: a mixture of 0.1 g of C1 (0.15 mmol), 20 cm^3 of N,N′-dimethylformamide, 0.0041 g 1-hydroxybenzotriazole hydrate, 0.052 cm^3 diisopropylethylamine, 0.8 g of BEN_APTES or PCH_APTES and 0.026 cm^3 of 1,3-diisopropylcarbodiimine in 30 cm^3 of chloroform [23] was stirred at room temperature for 15 h. The materials were separated by filtration, washed with 40 cm^3 of chloroform one time, with 40 cm^3 of N,N′-dimethylformamide twice, and again with 40 cm^3 of chloroform; they were dried at 120 °C overnight. The final materials are denoted as C1@ BEN_APTES and C1@ PCH_APTES.

2.3 Characterisation Methods

The Mn content was determined by atomic absorption spectroscopy (AAS) in a Pye Unicam SP9 spectrometer. Typically one sample of 20 mg of solid, previously dried at 100 °C, was mixed with 2 cm^3 of *aqua regia* and 3 cm^3 of HF (Riedel-de-Haën, 48%) for 2 h at 120 °C, in a stainless steel autoclave equipped with a polyethylene-covered beaker (ILC B240). After reaching room temperature the solution was mixed with about 2 g of boric acid (Fluka, 99, 9%) and finally adjusted to a known volume with deionised water.

XPS was performed at "Centro de Materiais da Universidade do Porto" (Portugal), in a VG Scientific ESCALAB 200A spectrometer using non-monochromatised Al Kα radiation. All the materials were compressed into pellets prior to the XPS studies. In order to correct possible deviations caused by electric change of the samples, the C 1 s line at 285.0 eV was used as the binding energy reference. The XPS spectra were fitted using a Gaussian–Lorentzian line shape, Shirley background [24, 25] and damped non-linear least-squares procedure. The line width of peaks (full width at half maximum—fwhm) was optimised for all components in individual spectra.

The FTIR spectra of diluted powders (4% in KBr, Sigma–Aldrich, spectroscopic grade) were obtained in the range of 4,000–400 cm^{-1}, with a Jasco FT/IR-460 Plus spectrophotometer; all spectra were collected with a resolution of 4 cm^{-1} and 256 scans.

The powder X-ray diffractograms were obtained in a Philips PX 1730 diffractometer using Cu Kα radiation. Oriented mounts were prepared by the powders deposition in glass slides after dispersion under sonication. In the case of the PCH based materials, diffraction peaks were not detected. This experimental fact was already mentioned in the literature [18, 25] and is due to the poor long range order that PCHs usually present.

The specific surface areas, micro and mesoporous volumes were obtained by the BET and *t*-method, respectively, [26] from nitrogen adsorption isotherms at −196 °C determined in an automatic apparatus Micromeritics, ASAP 2010. Before the measurements, the samples were outgassed in vacuum at 150 °C for 2.5 h.

The GC-FID chromatograms were obtained with a Varian CP-3380 gas chromatograph using helium as carrier gas and: (i) a fused silica Varian Chrompack capillary column CP-Sil 8 CB Low Bleed/MS (30 m × 0.25 mm i.d.; 0.25 μm film thickness) or (ii) a fused silica Varian Chrompack capillary column CP-Chiralsil-Dex CB (25 m × 0.25 mm i.d.; 0.25 μm film thickness) for quantification of enantiomeric excesses (ee) of the epoxides. Temperature program for alkenes epoxidation reactions: 60 °C for 3 min, increase of temperature at 5 °C min^{-1} until 170 °C; wait at this temperature for 2 min and then increase at 20 °C $min^{-1}$to 200 °C and finally stay at this temperature for 10 min; injector temperature, 200 °C; detector temperature, 300 °C. The peaks assignment of the catalytic reaction products was performed by comparison with commercial samples.

2.4 Catalytic Experiments

The activity of the catalysts in the epoxidation of alkenes was studied at 0 °C (ice bath) under constant stirring and using the following reagents quantities: 0.500 mmol of sty or ∝-Mesty (substrate), 0.500 mmol of chlorobenzene (GC internal standard) and 0.100 g of heterogeneous catalyst in 5.00 cm^3 of dichloromethane. Because substrates used show different reactivities towards the oxidants, different experimental conditions were used. For NaOCl reactions the substrate:NaOCl ratio was 2:3, [5] for *m*-CPBA reactions combined with NMO the substrate:*m*-CPBA:NMO ratio was 1:2:5 [27–29]. When the oxidant was NaOCl, the solution was buffered to pH 11 (Na_2HPO_4 + NaOH), to minimise formation of chlorinated products [30]. During the catalytic experiment 0.1 cm^3 aliquots were taken from the reaction medium, with a hypodermic syringe, filtered through 0.2 μm syringe filters, and directly analysed by GC-FID. After the essay, the catalysts were sequentially extracted/centrifuged 3 × 10 cm^3 of methanol and 3 × 10 cm^3 of dichloromethane and then dried in an oven at 100 °C overnight, and characterised by FTIR and N_2 adsorption isotherms. The catalytic reactions were also performed under similar conditions using APTES-functionalised supports without any

added complex: in all cases no significant substrate conversions were observed and no ee were detected.

The reaction parameters alkene conversion (%C), epoxide selectivity ($\%S_{epoxide}$), turnover number (TON), turnover frequency (TOF) and %ee were calculated using the following formula, where A stands for chromatographic peak area: $\%C = \{[A(alkene)/A(chlorobenzene)]_{t=0h}\text{-}[A(alkene)/A(chlorobenzene)]_{t=xh}\} \times 100/[A(alkene)/A(chlorobenzene)]_{t=0h}$, $\%S_{epoxide} = A(epoxide) \times 100/[A(epoxide) + \sum A(other\ reaction\ products)]$, $TON = \%C \times \%S_{epoxide} \times n(alkene)_{t=0h}/n(Mn)$, $TOF = TON/reaction\ time$ and $\%ee = [A(major\ enantiomer)\text{-}A(minor\ enantiomer)] \times 100/[A(major\ enantiomer) + A(minor\ enantiomer)]$.

3 Results and Discussion

3.1 FTIR Spectroscopy

Figures 1a, b show the FTIR spectra of the parent and organo-modified clay materials in the relevant region of 2,000–500 cm^{-1}. In the high energy range of 4,000–2,000 cm^{-1} (not shown) the FTIR spectrum of BEN has the typical intense and large bands at 3,620 cm^{-1} assigned to the surface hydroxyl groups from Al–OH and Si–OH stretching vibrations and bands at 3,410 cm^{-1} due to hydrogen bonded O–H stretching vibrations. Similarly, the FTIR spectrum of PCH shows a very broad, unsymmetrical band at about 3,400 cm^{-1}, which is composed by at least the two overlapping components observed in BEN spectrum. In the 2,000–500 cm^{-1} region both clay materials show a band attributed to physisorbed water in the range of 1,630–1,640 cm^{-1}, as well as bands assigned to clay lattice vibrations around 1,080 cm^{-1} due to asymmetric stretching of Si–O–Si linkage of the SiO_4 tetrahedra, around 950 cm^{-1} due to Si–OH stretching vibrations and around 802 cm^{-1} assigned to O–Si–O stretching.

The FTIR spectra of BEN_APTES and PCH_APTES show, besides the typical vibration bands attributed to the parent clay materials, new bands in the high energy range of 3,000–2,800 cm^{-1} (not shown) due to asymmetric and symmetric vibrations of CH_2 units from grafted APTES [30–32]. Additional evidence for the APTES functionalisation can be gathered from the appearance of bands in the 1,630–1,020 cm^{-1} region, Fig. 1, assigned to C–H and NH_2 bending vibrations of the grafted APTES [33, 34]. The band at 730 cm^{-1} is usually attributed to NH_2 coupled with Si–C stretching vibrations; [35] the peak at 695 cm^{-1} is due to overlapped CH_2 and Si–O vibrations [36].

Upon the clays modification, the intensity of the peak due to physisorbed water (in the range 1,630–1,640 cm^{-1}) decreases with broadening. The intensity decrease is the result of the decrease of the amount of physisorbed water in the clay lattice as a consequence of APTES grafting reaction between the organosilane ethoxyl groups and the clays surface hydroxyl groups. The broadening effect may be due to the overlapping of new bands at *ca.* 1,600 cm^{-1} characteristic of NH_2 bending vibrations of APTES [37] and vibrations of protonated amines (NH_3^+ group) around 1,610 cm^{-1}, eventually formed during the APTES grafting reaction [37].

The FTIR spectrum of C1@BEN_APTES (Fig. 1a) shows some changes compared to BEN_APTES material. A new asymmetric band centred at 1,658 cm^{-1} appears, composed by at least two bands, one at 1,634 cm^{-1} assigned to physisorbed water, and other at 1,658 cm^{-1} which can be

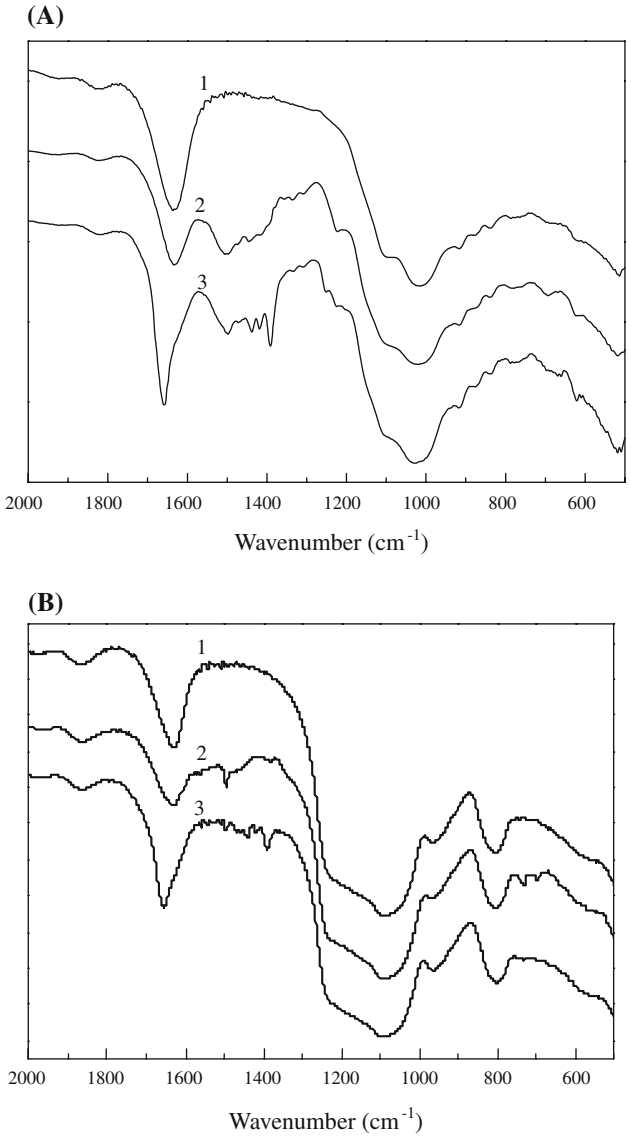

Fig. 1 FTIR spectra of the parent materials, organo-modified and with anchored complex C1 in the 2000–500 cm^{-1} region: (**a**) *1* BEN, *2* BEN_APTES, *3* C1@BEN_APTES; (**b**) *1* PCH, *2* PCH_APTES, *3* C1@PCH_APTES

due to the C=O and C=N stretching vibrations from the anchored C1 complex. Moreover, new weak bands are observed at 1,438, 1,418, 1,391 and 1,211 cm^{-1} that can be assigned to the anchored complex, since their frequencies are quite similar to those of the free complex [22]. The changes in the FTIR spectrum of C1@PCH_APTES are similar to those observed for C1@BEN_APTES, although with less intensity, anticipating that the complex anchored in this material is in lower quantity: the FTIR spectrum shows a new asymmetric band centred at 1,655 cm^{-1} and also new vibrations at 1,439 and 1,389 cm^{-1} confirming the immobilisation of C1 in PCH material. Both spectra are relatively unchanged in the 1,000–500 cm^{-1} region, confirming that C1 has been successfully grafted onto BEN_APTES and PCH_APTES without significant changes in the clays structure.

3.2 XPS

In Table 1 is summarised the surface elemental composition of all the BEN and PCH based materials obtained by XPS; the core level binding energies and fwhm obtained by deconvolution of the XPS high-resolution spectra are presented in Table S1, Supplementary Material.

The high-resolution XPS spectra of the original materials show a band in the Si 2p region corresponding to silicon from the clay tetrahedral sheets. For PCH this band is asymmetric, with the less intense component at 100.0 eV being assigned to colloidal silica [38]. In the O 1 s region, both materials show a symmetric band at 532.3 eV for BEN and 533.2 eV for PCH due to single bonded oxygen from the clays lattice. A band centred at 74.9 eV (BEN) and 73.8 eV (PCH) is observed in the Al 2p region, which is due to Al^{3+} cations in the clay sheets. Moreover, in the C 1 s region low intensity bands are observed at 285.0 eV and 287.6 eV due to impurities.

The grafting of APTES onto BEN and PCH leads to an increase in the carbon and nitrogen surface contents and a decrease in the oxygen content, Table 1. The high-resolution spectra of both functionalised materials show an asymmetric band in the C 1 s region which can be deconvoluted into three components: two peaks at 285.0 and 288.3–287.9 eV due to carbon already present in the parent materials (impurities) and an additional band at 286.5–286.0 eV which can be attributed to C–N from APTES [39, 40]. Moreover, the peaks at 400.0 and at 402.3–402.0 eV in the N 1 s region are attributed to $–NH_2$ and protonated amine groups, respectively, [37].

The material C1@BEN_APTES reveals, besides the elements already present in the parent material, the existence of manganese and chlorine elements due to the anchored Mn complex; the complex immobilisation also induce an increase in the atomic % of carbon and nitrogen. The Al/Si ratio in C1@BEN_APTES is the same as in the parent and APTES modified BEN, confirming that no disruption of the clay structure took place upon the complex immobilisation. The comparison of Mn content obtained from XPS and AAS (surface vs. bulk contents, Table 2) suggests that the complex is mainly anchored onto the support external surface, since the surface content (67 μmol g^{-1}) is higher that the bulk one (27 μmol g^{-1}); this is an expected results since APTES functionalisation occurs at the surface hydroxyls groups located at the edges of the clays layers, and thus the complex is anchored through the grafted spacer [40].

The material C1@PCH_APTES show very small atomic % of manganese and to chlorine (that were unable to simulate, see Table S1), besides de other elements already present, what anticipates a lower surface content of Mn complex in this material compared with the C1@BEN_APTES. In this material the complex immobilisation also leads to an increase in nitrogen and carbon atomic %, although in this latter value the % increase is much higher than that expected from complex anchoring, which is probably a consequence of an organic contamination The Mn content was determined by AAS, Table 2, and the obtained value of 2 μmol g^{-1} confirms that in fact a smaller amount of complex has been anchored within PCH when compared with BEN parent materials. The comparison between surface (16 μmol g^{-1}) *vs* bulk (2 μmol g^{-1}) Mn contents, Table 2, suggests that the

Table 1 Atomic percentages of selected elements obtained by XPS for clay based materials

Material	Atomic %										
	C 1 s	N 1 s	O 1 s	Mg 1 s	Al 2p	Si 2p	Cl 2p	Mn $2p_{3/2}$	Fe 2p	Al/Si	Mn/Si
BEN	9.5	0.3	56.8	2.0	6.7	23.5			1.1	0.3	
BEN_APTES	14.2	2.2	54.6	2.0	5.6	21.1			0.4	0.3	
C1@BEN_APTES	20.7	3.0	47.3	1.4	5.8	20.5	0.2	0.1	0.9	0.3	0.005
PCH	9.4	0.9	57.5	0.3	0.3	31.5			0.1	0.01	
PCH_APTES	7.5	2.2	57.7	0.1	0.6	31.7			0.1	0.02	
C1@PCH_APTES	22.3	2.7	45.3	0.1	0.6	28.8	0.03[a]	0.03[a]	0.1	0.02	0.001

[a] Estimated from very small intense signals

Table 2 Bulk and surface Mn contents determined by AAS and XPS, before and after catalytic tests

Material	Conditions: Substrate/oxidant	Mn content (μmol g^{-1})		
		AAS		XPS[a]
		Before	After	Before
C1@BEN_APTES		27		67
	α-Mesty/NaOCl		11	
	sty/*m*-CPBA		28	
	α-Mesty/*m*-CPBA		12	
C1@PCH_APTES		2		16
	α-Mesty/NaOCl		[b]	
	sty/*m*-CPBA		3	
	α-Mesty/*m*-CPBA		3	

[a] Mn surface content per weight of sample (before catalytic tests) calculated from XPS data in Table 1: μmol Mn/weight of sample = atomic % Mn/[atomic % C × Ar(C) + atomic % N × Ar(N) + atomic % O × Ar(O) + atomic % Mg × Ar(Mg) + atomic % Si × Ar(Si) + atomic % Al × Ar(Al) + atomic % Cl × Ar(Cl) + atomic % Mn × Ar(Mn) + at% Fe × Ar(Fe)]

[b] Mn content below the AAS analysis detection limit

complex is anchored in the material outer pores. The low complex bulk content in PCH compared to BEN and the fact that surface is higher than the bulk contents suggest the existence of pore diffusion constraints to complex immobilisation within PCH pores, induced by some pore blocking caused by APTES grafting (see below in 3.3 section). Similarly to BEN based material, the Al/Si ratio in C1@PCH_APTES is the same as in the parent and APTES modified PCH, confirming that no disruption of the material structure took place upon the complex anchoring.

3.3 Textural Properties

When comparing the X-ray diffractograms of the parent BEN and BEN_APTES samples, Fig. 2, it is possible to observe that the peak assigned to the basal spacing (d_{001}) which is initially near $2 = 6^{\circ}$ (curve 1) is shifted to lower 2 values (curve 2). This can be interpreted as a result of the APTES grafting not only in the clay sheets borders but also in the clay interlayer region at least in some extension, leading to some degree of expansion of the interlayer region. A similar situation was also reported in the literature for other types of montmorillonite clays [41]. Furthermore, a further shift to low 2 values is observed after complex anchoring (curve 3). The peaks in curves 2 and 3 are broader than that of the initial BEN, as a consequence of higher heterogeneity of the basal spacing among various clay crystallites.

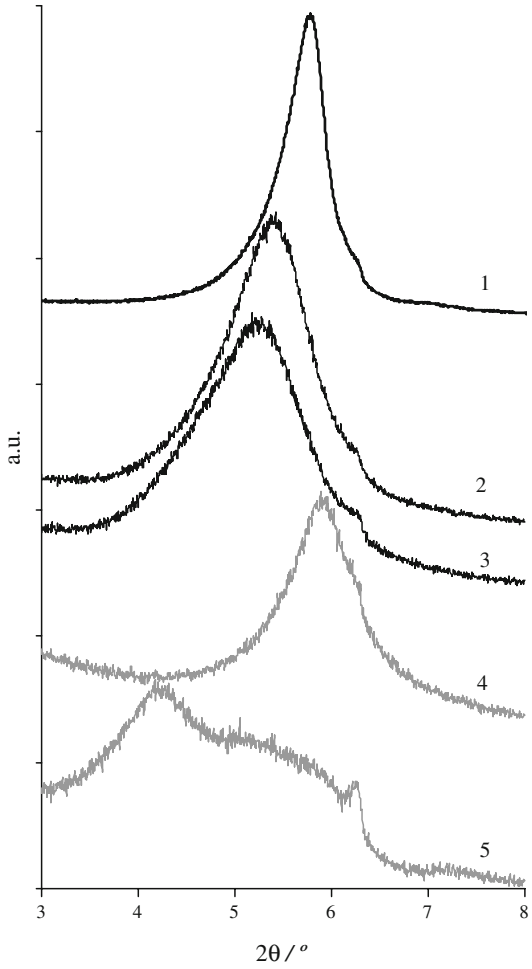

Fig. 2 X-ray diffractograms of BEN based materials: *1* BEN, *2* BEN_APTES, *3* C1@BEN_APTES. The curves 4 and 5 stand for C1@BEN_APTES after the catalytic reaction with α-Mesty/NaOCl and α-Mesty/*m*-CPBA/NMO, respectively

The N_2 adsorption isotherms at −196 °C are given in Fig. 3a for BEN based samples. As expected, and already discussed in the literature, [42] the curve for the parent BEN (curve 1) is essentially a curve typical for a non-porous material, as revealed also by the low specific surface area of 37 m^2 g^{-1}, Table 3. The observed desorption hysteresis is mainly due to the adsorption in spaces formed by the aggregation of the clay micro-particles. After modification of the BEN material with APTES and C1, the specific surface area is successively reduced as a consequence of the different arrangements in the crystallite aggregates, as already reported for other clays [41]. In fact, the very low surface area of the sample with the complex (see Table 3), precluded the accurate determination of the complete adsorption isotherm for this sample.

In the case of the PCH based materials (Fig. 3b), the isotherm is of a mixed type I + II, according to the IUPAC classification, [26] due to the types of porosity of PCHs,

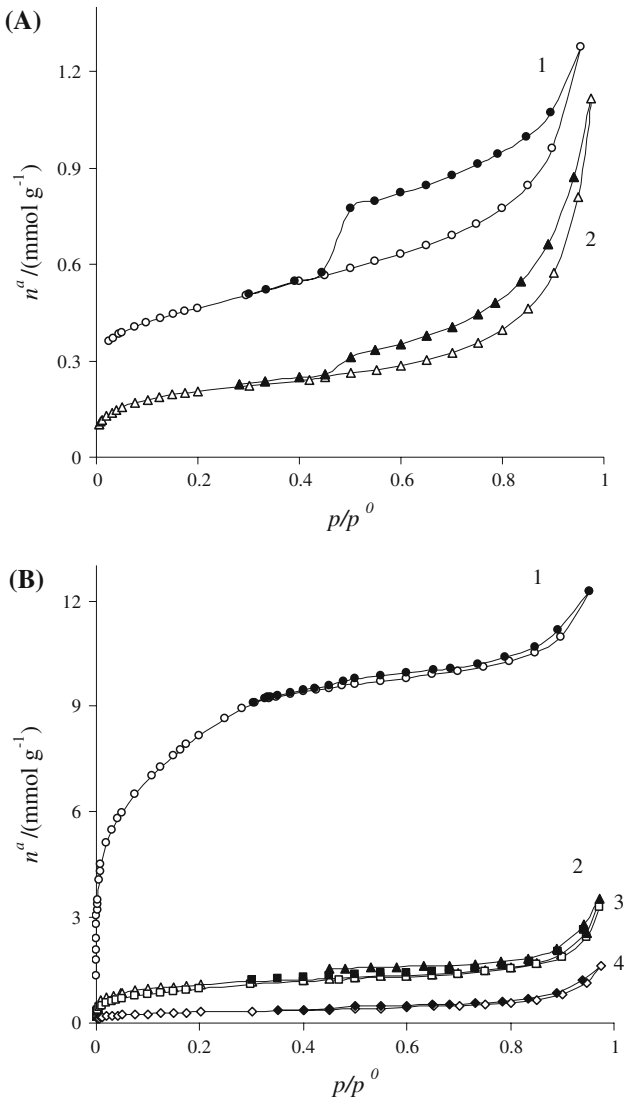

Fig. 3 Nitrogen adsorption isotherms at −196 °C of (**a**): *1* BEN, *2* BEN_APTES, and (**b**): *1* PCH, *2* PCH_APTES, *3* C1@PCH_APTES. The curve 4 in (**b**) stands for C1@PCH_APTES after the catalytic reaction of α-Mesty/NaOCl. Open symbols (*open circle*), adsorption; solid symbols (*closed circle*), desorption

Table 3 Specific surface areas (A_{BET}), microporous volumes (V_{micro}) and mesoporous volumes (V_{meso}) estimated from the nitrogen adsorption isoterms at −196 °C

Material	A_{BET} (m^2 g^{-1})	V_{micro} (cm^3 g^{-1})	V_{meso} (cm^3 g^{-1})
BEN	37		
BEN_APTES	17		
C1@BEN_APTES	9		
PCH	605	0.29	0.14
PCH_APTES	88	0.02	0.09
C1@PCH_APTES	81	0.03	0.11

which present micro and mesopores and for which the porosity is in the transition region between micro and mesopores [42]. The modification with APTES clearly reduces the available porosity of the sample (curve 2). In fact, the total porosity (micro + mesopores) is reduced to about 1/3 of the initial value. Further reduction is observed upon the complex anchorage.

3.4 Catalytic Activity

The catalytic activity of the new materials was tested in the epoxidation of sty and α-Mesty, using NaOCl and *m*-CPBA/NMO as oxygen sources; the results are summarised in Table 4.

Under the experimental conditions used it is possible to see that the catalyst C1@BEN_APTES has a very low substrate conversion when NaOCl is used as the oxidant, but for all the other conditions C1@BEN_APTES and C1@PCH_APTES are active in the epoxidation reactions of the two alkenes, although with %C in the range of 14–33%. Moreover, all the catalysts show high epoxide selectivities, 71–84% (except for reactions using NaOCl as oxygen source), but exhibit low %ee. In general, the epoxidation of sty with *m*-CPBA/NMO as the oxidant system reaches the maximum of substrate conversion faster than with α-Mesty for both catalysts. In terms of substrate conversions and selectivities, when using the *m*-CPBA/NMO, the C1@PCH_APTES catalyst presents higher sty conversion and epoxide selectivity than the C1@BEN_APTES counterpart, but with α-Mesty substrate the opposite tendency is observed with the latter catalyst being the most efficient one. To the best of our knowledge, there is only one example in literature that can be directly compared with our results: the complex was immobilized in HMS using the same anchoring methodology, [21] and tested in the enantioselective epoxidation of *m*-CPBA/NMO. Although the reaction time was 4 h, only 1% was obtained for ee% value. This complex was also immobilized through a similar spacer into an organic polymer, but its catalytic activity was tested using a more reactive substrate (6-cyano-2,2-dimethylchromene) in conjunction with *m*-CPBA/NMO, leading to higher substrate conversion % (72%) and higher ee% (86%) [43].

The catalytic reactions using C1@PCH_APTES have longer reaction times than C1@BEN_APTES, probably as a consequence of the lower Mn content of the former catalyst. It is worthwhile to mention that, even though C1@PCH_APTES has much lower Mn content than C1@BEN_APTES, their %C are of the same magnitude, and consequently the TON and TOF values are much higher for the former catalyst, suggesting that the immobilised C1 in PCH behaves as a more efficient catalyst.

Table 4 Enantioselective epoxidation of Sty and α-Mesty catalysed by immobilised C1[a]

Material	Substrate	Oxidant	t^b (h)	%C[c]	Epoxide[c]		Others[c]		%ee	TON	TOF (h^{-1})
					%S	%Y[d]	%S	%Y[d]			
C1@BEN_APTES	α-Mesty	NaOCl	5	2	19	1	81	1	65	1	0.2
	α-Mesty	*m*-CPBA	9	29	80	23	20	6	3	4	0.4
	Sty[e]	*m*-CPBA	6	14	71	10	29	4	5	18	3
C1@PCH_APTES	α-Mesty	NaOCl	24	15	16	2	84	13	14	211	9
	α-Mesty	*m*-CPBA	24	18	74	14	26	5	6	512	21
	Sty[f]	*m*-CPBA	9	33	84	28	16	5	6	1,066	119

[a] Molar ratio α-Mesty/NaOCl = 2:3; Molar ratio substrate/*m*-CPBA/NMO = 1:2:5

[b] Reaction time at which the substrate conversion start to become constant

[c] Determined by GC against internal standard

[d] $\%Y$ = yield % and calculated as $\%C \times \%S/100$

[e] No benzaldehyde was detected in the products

[f] $\%S$ of benzaldehyde = 0.8, $\%Y$ of benzaldehyde = 0.25

At the end of the catalytic tests the catalysts were further characterised by Mn-AAS, FTIR, PXRD (for BEN based catalyst) and N_2 adsorption isotherms. The Mn contents in Table 2 show that for C1@BEN_APTES there was approximately 40% complex leaching upon reactions using the catalytic systems α-Mesty/NaOCl and α-Mesty/*m*-CPBA/NMO, but no leaching was observed for sty/*m*-CPBA/NMO. Therefore the higher %C of the C1@BEN_APTES in the α-Mesty epoxidation with *m*-CPBA/NMO may have a contribution of leached compplex.

For C1@PCH_APTES the Mn content of the catalyst after the α-Mesty epoxidation with NaOCl oxidant was below the detection limit of the technique, suggesting some % of complex leaching, but for the other catalytic systems the Mn contents are similar to that obtained before catalysis.

The comparison of the FTIR spectra of C1@BEN_APTES before and after the catalytic reactions (Figure S1—A, Supplementary Material) suggests some metal complex decomposition (some broadening of the vibration bands assigned to the complex), probably by partial oxidation under the catalytic experimental conditions used [43]. When NaOCl was used as oxidant some changes in the bands assigned to the clay structure are also detected. Furthermore, new bands at 1,356 and 860 cm^{-1} are detected in the FTIR spectrum of the recovered catalyst after the reaction with α-Mesty/NaOCl system (Figure S1—A, Supplementary Material), indicating the presence of occluded epoxide species which have not been removed during the washing process. These facts can be confirmed by the diffractograms in Fig. 2 obtained with materials after the catalytic reaction with α-Mesty/NaOCl and α-Mesty/*m*-CPBA/NMO, curves 4 and 5, respectively. When NaOCl was used, the diffractogram is more similar to that of the initial BEN material, suggesting that a significant part of the APTES and complex have been leached; this can be due to the pernicious effect of high pH used in the experimental catalytic procedure. In the case of the *m*-CPBA/NMO oxidant system, the changes in the diffractogram (curve 5) are more intricate: the broadness of the peak suggests the occurrence of two simultaneous effects: the leaching of the organic parts, which lead to the displacement of the peak to high 2 values, and the retention of reaction products in the interlayer region, expanding the layers, and being responsible for the shift for low 2 values.

The FTIR spectrum of the recovered C1@PCH_APTES used in the reaction with NaOCl (Figure S1—B, Supplementary Material) confirms the complex leaching and damage of the spacer structure since the complex and APTES vibration bands are not detected. When *m*-CPBA/NMO was used as oxidant, the FTIR spectra of the recovered C1@PCH_APTES materials are similar to that of the as-prepared catalyst, suggesting that the complex remained within the material, sustaining the Mn-AAS data.

The characterisation of the recovered catalysts showed that although BEN_APTES anchored C1 in higher percentage, it acted as a less stable support than the PCH counterpart under the catalytic epoxidation conditions used.

4 Conclusions

The functionalisation of a natural clay and a porous clay heterostructure with APTES was succeeded and both organo-modified clays were able to anchor Mn(III) salen complex C1, although with higher efficiency for the natural clay (C1@BEN_APTES) than for the porous clay heterostructure (C1@PCH_APTES).

Both C1@BEN_APTES and C1@PCH_APTES materials acted as moderate catalysts (although with low ee%) in the epoxidation of styrene and α-methylstyrene with two different oxidant sources, NaOCl and *m*-CPBA/NMO. The C1@PCH_APTES catalyst showed higher catalytic activity in terms of alkene conversion as well as epoxide yield when styrene was the substrate in combination with *m*-CPBA/NMO.

The oxidising systems used had some destructive effect in the hybrid catalysts. Although the situation is not entirely clear, some major effects can be pointed out. In the case of the BEN based material, the deleterious effect of NaOCl on the support seems to act at the level of the active phase leaching and on the structure support damaging, and may be related with the strong alkaline conditions necessary to perform the catalytic reactions. In the case of the *m*-CPBA/NMO system, the C1 leaching was less extensive and a minor structural damage of the support also occurred. For PCH based catalyst, similar pernicious effect of NaOCl in the support was also observed, but for the other oxidising system no significant effects were detected both in the immobilised complex and support structure.

Finally, it must be emphasised that a successful complex immobilisation must involve not only the efficiency of the immobilisation strategy, but also the stability of the resulting material (support and complex) under the experimental catalytic reaction conditions. This study showed that epoxidation reactions using NaOCl as oxygen source should be avoided when using clay based materials as supports for Mn(salen) catalysts, highlighting the importance of a careful choice of the oxidant source in each catalytic reaction. Nevertheless, porous clay heterostructures should be considered as promising supports for metal complexes with catalytic properties.

Acknowledgments This work was funded by Fundação para a Ciência e a Tecnologia (FCT) and FEDER, through project ref. PPCDT/CTM/56192/2004. IKB thanks FCT for a Post-Doctoral fellowship.

References

1. Smith K, Liu CH (2002) Chem Commun 886
2. Canali L, Cowan F, Deleuze H, Gibson CL, Sherrington DC (2000) J Chem Soc., Perkin Trans 1:2055
3. Zhang H, Zhang Y, Li C (2005) Tetrahedron Asymmetr 16:2417
4. Zhang H, Xiang S, Ciao J, Li C (2005) J Mol Catal A: Chem 238:175
5. Park DW, Choi SD, Choi SJ, Lee CY, Kim GJ (2002) Catal Lett 78:145
6. Kureshy RI, Khan NH, Abdi SHR, Ahmad I, Singh S, Jasra RV (2004) J Catal 221:234
7. Bhattacharjee S, Dines TJ, Anderson JA (2004) J Catal 225:398
8. Das P, Kuźniarska-Biernacka I, Silva AR, Carvalho AP, Pires J, Freire C (2006) J Mol Catal A: Chem 248:135
9. Xiang S, Zhang Y, Xin Q, Li C (2002) Chem Commun 2696
10. Zhang H, Zhang Y, Li C (2005) Chem Commun 1209
11. Zhang H, Li C (2006) Tetrahedron 62:6640
12. Kureshy RI, Ahmad I, Khan NH, Abdi SHR, Pathak K, Jasra RV (2006) J Catal 238:134
13. Zhang H, Meng Y, Wang L, Zhang G, Gerritsen HCL, Abbenhuis RA, van Santen RA, Li C (2008) J Catal 256:226
14. Kuźniarska-Biernacka I, Silva AR, Ferreira R, Carvalho AP, Pires J, Brotas de Carvalho M, Freire C, de Castro B (2004) New J Chem 28:853
15. Gil A, Gandía LM, Vicente MA (2000) Catal Rev Sci Eng 42:145
16. Tanev PT, Pinnavaia TJ (1995) Science 267:865
17. de Stefanis A, Tomlinson AAG (2006) Catal Today 114:126
18. Pires J, Araújo AC, Carvalho AP, Pinto ML, González-Calbet JM, Ramírez-Castellanos J (2004) Micropor Mesopor Mater 73:175
19. Ray SS, Okamoto M (2003) Prog Polym Sci 28:1539
20. Stretza HA, Paula DR, Lib R, Keskkulaa H, Cassidy PE (2005) Polymer 46:2621
21. Silva AR, Wilson K, Clark JH, Freire C (2006) Micropor Mesopor Mater 91:128
22. Guil JM, Perdigón-Melón JA, de Carvalho MB, Carvalho AP, Pires J (2002) Micropor Mesopor Mater 51:145
23. Song CE, Roh EJ, Yu BM, Chi DY, Kim SC, Lee K-J (2000) Chem Commun 615
24. Shirley DA (1972) Phys Rev B 5:4706
25. Zhu HY, Ding Z, Barry JC (2002) J Phys Chem B 106:11420
26. Rouquerol F, Rouquerol J, Sing K (1999) Adsorption by Powders & Porous Solids. Academic Press, London
27. Palucki M, Pospisil PJ, Zhang W, Jacobsen EN (1994) J Am Chem Soc 116:9333
28. Fan Q-H, Li Y-M, Chan ASC (2002) Chem Rev 102:3385
29. Zhang W, Jacobsen EN (1991) J Org Chem 56:2296
30. Zheng S, Gao L, Guo J (2001) Mater Chem Phys 71:174
31. Etienne M, Walcarius A (2003) Talanta 59:1173
32. Bourlinos AB, Jiang DD, Giannelis EP (2004) Chem Mater 16:2404
33. White LD, Tripp CP (2000) J Colloid Interface Sci 232:400
34. Bistričić L, Volovšek V, Dananić V (2007) J Mol Struct 355: 834–836
35. Peña-Alonso R, Rubio F, Rubio J, Oteo JL (2007) J Mater Sci 42:595
36. Chong ASM, Zhao XS (2003) J Phys Chem B 107:12650
37. Zhao D, Yang Y, Guo X (1992) Inorg Chem 31:4727
38. Matuana LM, Balatinecz JJ, Park CB, Sodhi RNS (1999) Wood Sci Technol 33:259
39. Pereira C, Patrício S, Silva AR, Magalhães AL, Carvalho AP, Pires J, Freire C (2007) J Colloid Interface Sci 316:570
40. Carvalho MB, Pires J, Carvalho AP (1996) Micropor Mater 6:65
41. Pires J, Pinto M, Estella J, Echeverría JC (2008) J Colloid Interface Sci 317:206
42. Fraile JM, García JI, Massam J, Mayoral JA (1998) J Mol Catal A:Chem 136:47
43. Song CE, Roh EJ, Yu BM, Chi DY, Kim SC, Lee K-J (2000) Chem Comm 615